JMEPEG (2012) 21:1703–1707
DOI: 10.1007/s11665-011-0096-9

1059-9495/$19.00

Compressive Behavior of Conductive Graphite Foams

C.E. Smith, A.L. Gyekenyesi, M. Singh, and *J. Bail*

(Submitted October 6, 2011)

This study describes the compressive mechanical properties of graphite foam as a function of relative density. Reported data include strengths, moduli, and a description of the damage progression. The compressive strength, as a function of density, exhibited good agreement with existing, empirical foam models. In addition, optical strain data provided insight into the damage evolution. Failure was observed to occur due to localized density variations that allowed for the weaker (i.e., less dense) layers to successively fail with increasing load. Note that this particular material is deemed "developmental" in that it is not yet commercially available and the processing conditions are still being optimized. Finally, detailed mechanical data is lacking for this class of material, and as a result, the properties and behavior reported here will aid in optimizing manufacturing and design efforts.

Keywords advanced characterization, aerospace, mechanical testing

1. Introduction

Due to increased performance in a wide range of engineered products ranging from computer processors to advanced aerospace vehicles, there is a critical need for improved thermal management systems for transferring heat. The required enhancements include increased thermal conductivity, increased surface area, reduced weight/volume, as well as operability in harsh environments (e.g., durability under high flow rates, vibrations, stress, elevated temperatures, and oxidative environments). Graphite foams are excellent candidates for thermal management applications due to their extraordinary thermal characteristics and large surface area (Ref 1, 2). Graphite foams have reported ligament conductivities greater than 1800 W/m·K and bulk values up to 245 W/m·K (as a comparison, fully dense aluminum = 180 W/m·K). An extensive review of graphite foam development, prototype applications, as well as potential future uses have been discussed in Ref 2 and 3.

Before future heat exchangers can be designed with these relatively new foam materials, the mechanical properties must be well characterized. While data does exist for low conductivity glassy carbon foams used for insulation, there is currently minimal data available regarding the mechanical properties of thermally conductive graphite foams. The goal of this study is to understand the compressive strength and deformation behavior, especially as it relates to foam produced by GrafTech International Holdings, Inc. (GTIH: Parma, OH). An overview of the project and basic foam fabrication procedures are described in Ref 4.

C.E. Smith, A.L. Gyekenyesi, M. Singh, and **J. Bail**, Ohio Aerospace Institute, 22800 Cedar Point Road, Cleveland, OH 44142. Contact e-mail: craigsmith@oai.org.

2. Experimental Procedure

Standards for the mechanical testing of porous ceramics require that specimen dimensions equate to a minimum of 10 pores per side (Ref 5). Based on the pore size of the graphite foams tested here (cell sizes were approximately 0.6 mm: 0.02 in.), a minimum dimension of 7 mm (0.28 in.) was selected (Fig. 1). Rectangular samples of various length/width (L/W) ratios were first cut from a single billet to examine the effects of the L/W ratio on the mechanical properties. Specimen dimensions for mechanical testing of additional billets were then selected based upon this data.

Monotonic compressive tests were carried out using an electro-mechanical load frame with parallel compression anvils. Samples were centered on the bottom plate and the top plate was lowered until it nearly contacted the sample. Keeping with ASTM C1674 (Ref 5), the compressive load rate for the porous ceramic foam was chosen such that the peak load was reached within 30-50 s. Hence, a rate of 0.64 mm/min (0.025 in./min) was selected. Note that machined parallels were utilized to verify the alignment of the compression anvils.

The acquisition of accurate strain measurements was an early concern. Several methods of strain measurement were initially explored. The simplest way was to calculate strain based on the crosshead displacement. This provided a global strain encompassing the entire sample. The compliance of the fixture was also measured and subtracted from the final data. To assure accuracy, a check was made by utilizing a noncontact, laser extensometer. The approach optically tracked the displacement of two surface mounted flags on the specimen. In addition, a capacitance extensometer was used in contact with the compression anvils as a final verification of the crosshead displacement. Although detailed results regarding the comparison of these strain measurements are not presented in this article, it is sufficient to note that the crosshead displacement proved to be an accurate measure of global strain for the low loads experienced.

In addition, a full field optical strain measurement system was employed to study localized deformation behavior. The system consisted of two digital cameras arranged in stereo and connected to a computer with pattern recognition software. A

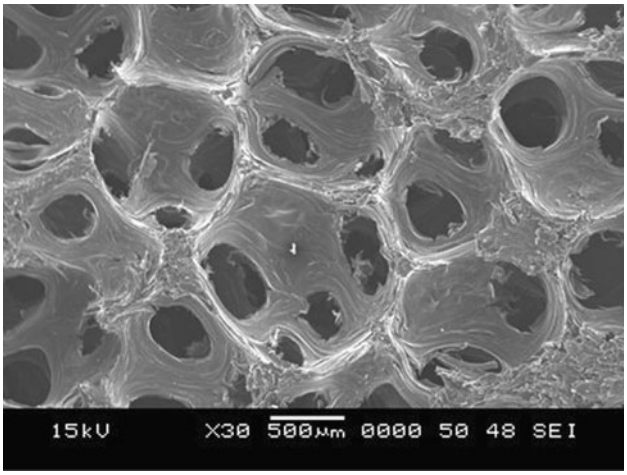

Fig. 1 Scanning electron microscopy image showing graphite foam cell morphology (Ref 9)

calibration process was performed to calculate and store the camera positions relative to each other. A random black and white speckle pattern was then applied to the test specimen using spray paint. The system used the pattern recognition software to compare the changing speckle pattern on the specimen under load from a series of images taken by the two cameras. The optical measurement system has a resolution of approximately 10^{-3} mm. The measured load was recorded by an analog input from the universal testing machine at the time of the captured picture and was used to generate a stress-strain curve.

Due to the manufacturing process, it is well known that the with-rise (WR) direction offers superior mechanical and thermal properties in comparison to the against-rise (AR) direction (Ref 1-3). The highly conductive graphite crystals preferentially align in the WR direction. In addition, processing may cause the pores to slightly elongate in the vertical/WR direction, adding to the anisotropy. Testing was done for both the WR and the AR orientations.

3. Results and Discussion

The graphite foam specimens had densities ranging from approximately 0.1 to 0.8 g/cm^3. Regarding the proper selection of the L/W ratio, the test results showed that the compressive strength had a large degree of scatter and no significant relationship to the selected L/W ratios (Fig. 2). While the average stiffness increased with greater L/W ratio, this was accompanied by increased scatter (i.e., heteroscedasticity). Based on these results and the dimensions used in previous studies (Ref 6), an L/W ratio of 2 was selected for all mechanical testing. Also, most of the graphite foam material provided for this effort was limited to 2.54 cm (1 in.) thick panels. Therefore, rectangular samples with dimensions 1.3 × 1.3 × 2.5 cm (½ × ½ × 1 in.) were used (Fig. 3).

Optical imaging provided insight concerning the damage progression. Figure 4(a) shows meshed pictures generated by the optical imaging system for a typical compression test (the pictures were selected from a continuous sequence/movie taken during the compression tests). The images indicated that the

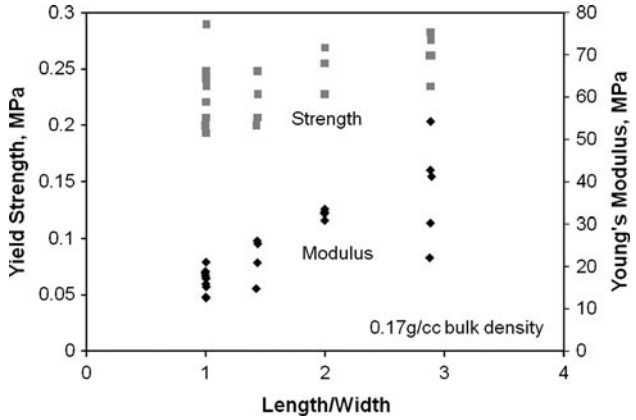

Fig. 2 Yield strength and Young's modulus versus length/width (L/W) ratio for samples tested in the with-rise (WR) direction

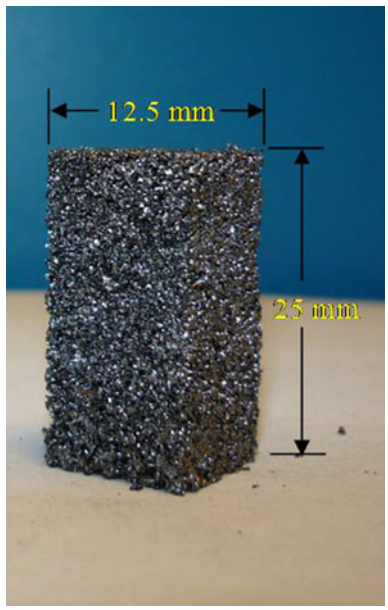

Fig. 3 Foam specimen dimensions utilized for compression experiments

material was uniformly strained up to approximately 0.5%. Beyond that point, the displacements became nonuniform with select regions showing large strains. Next, in order to compare the global strain calculated using crosshead displacements to the actual strains in the material, the relative displacements of the points labeled A and B (Fig. 4a) were used as a virtual, optical strain gage. Note that the optically based strain curve is offset by 0.7% so that the peak stresses of the two curves would correspond with one another. Also note that points A and B both lie outside the high strain region of Fig. 4(a).

The results in Fig. 4(b) show that the global strains exhibited a bi-linear behavior, with the material stiffening prior to 0.7%. This behavior was much less pronounced in the optical imaging data, which appeared to be very linear up to approximately 0.45 MPa. The fact that the two curves are nearly identical beyond the bi-linear region indicates that the deformation of the bulk material was the same as that of the local material up to the first peak stress. At the point of first peak stress, the local optical-based strain was 1.1%, while the

global strain-based on crosshead displacements was 1.8%. It was concluded that the initial bi-linear behavior observed mainly in the global data is likely the result of uneven loading among ligaments in contact with the load-frame's compression anvils due to the unevenness of the foam surfaces. Once all ligaments were contacted and the load became uniform, then the stiffness was constant and the local strain followed the global strain. Further loading beyond the first peak stress caused the global stress-strain curve to fluctuate about a plateau

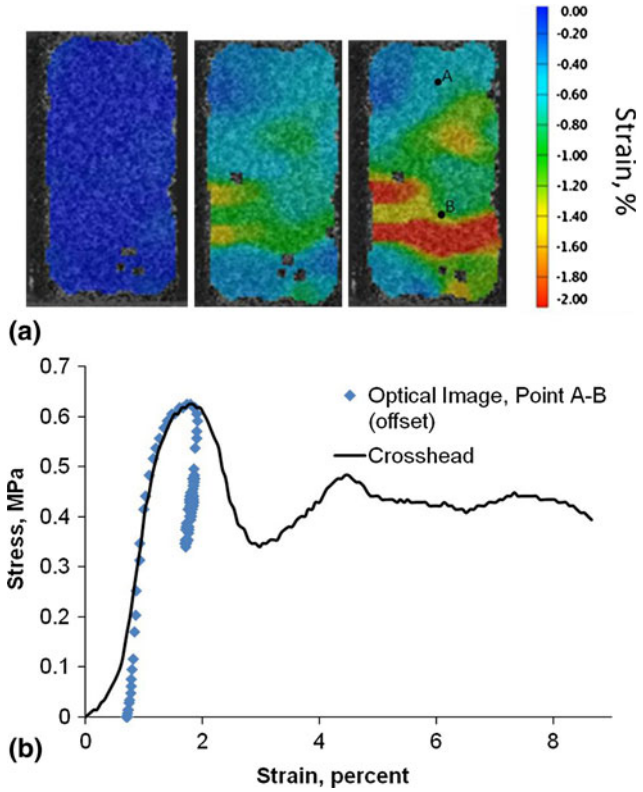

Fig. 4 (a) Select optical images taken from a movie sequence of a typical compression tests. (b) The stress-strain response calculated by the both crosshead displacement and virtual strain gage between points A and B from the optical images. Note that the curve for the optical image is offset by 0.7% for clarity

stress, similar to Fig. 5 and 6. In contrast, the local optical strain decreased beyond the peak stress. The subsequent stress peaks observed in the global material caused the local material to elastically deform and relax, as seen in the points at the end of the local stress-strain curve in Fig. 4(b). This is consistent with successive crushing of weak low density layers outside the optical strain gage section (i.e., remote of points A-B). As each layer crushed, it reduced the stress on the sample by allowing the un-crushed portion to relax elastically (the tests were conducted in stroke control). Brittle ceramic foams are also known to collapse by successive fracturing of cell edges (Ref 7).

Gibson and Ashby (Ref 8) have previously reported that the linear portion of the loading curve for open cell foam with a relative density of less than 0.1 (foam bulk density normalized by solid material density: solid graphite = 2.2 g/cc) is due primarily to ligament bending. For higher densities, ligament compression begins to play a role (the samples tested here had relative densities of 0.05-0.3). The optical imaging data reported here verifies that crushing/ligament fracture occurred successively, layer by layer. The strain field outside of the damaged/fractured layers was uniform and linear, and therefore a result of elastic ligament bending and compression. The optical imaging data also indicated that the global stiffness measured by the crosshead displacement (beyond the bi-linear region) corresponded well with the stiffness of the local, un-damaged foam.

Typical compressive stress-strain curves are presented in Fig. 5 to 7. Note that since densification takes place at approximately 80% strain, many samples in this study were interrupted prior to that point due to the excessive duration of the test. Each plot shows some degree of bi-linear behavior early on during initial load-up. The overall shapes of the curves in Fig. 5 are consistent with other porous foams (i.e., the stress increases to the point of cell crushing, at which time it flat-lines until the densification stress is reached). The same behavior was seen in certain WR samples as well. The WR samples that behaved similar to the AR samples (i.e., a fairly flat-line region after crush initiation) were those which had a high crushing strength for the given density (Fig. 6). WR samples that appeared to be relatively weak (those at densities above 0.5 g/cc) had a somewhat different stress-strain pattern. The first peak stress of these samples was low, but the continued crushing

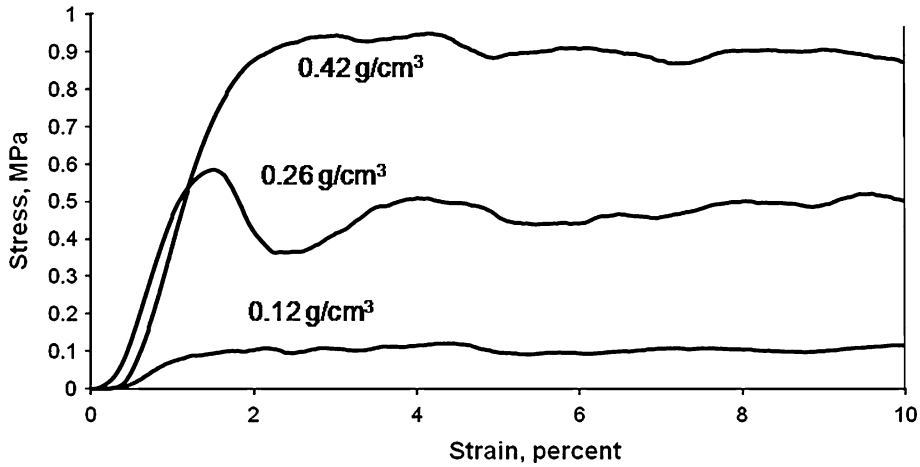

Fig. 5 Typical AR compressive stress-strain behaviors for select densities

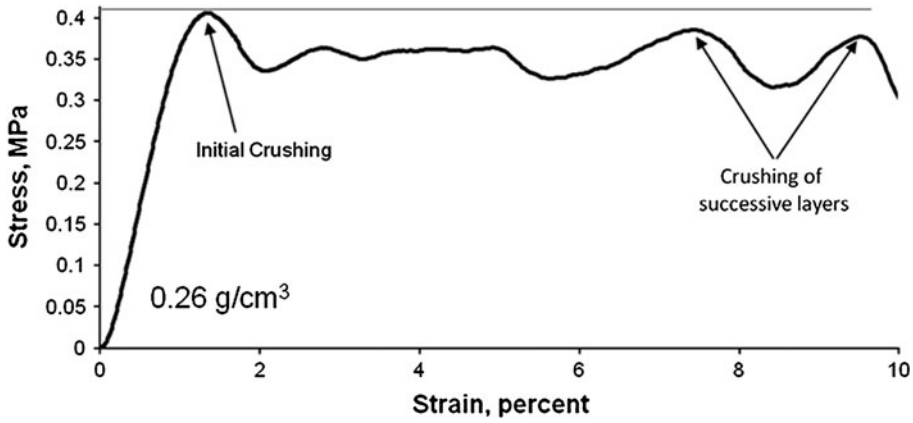

Fig. 6 Compressive stress-strain behavior for WR strong specimen

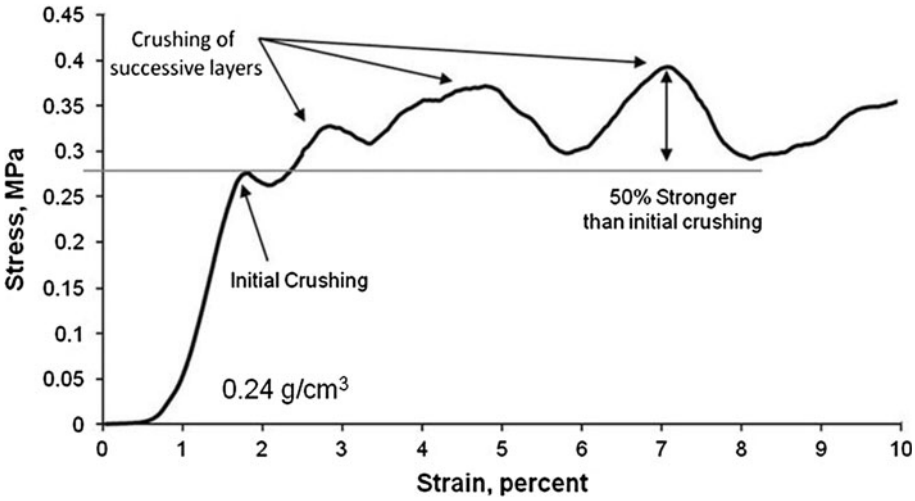

Fig. 7 Compressive stress-strain behavior for WR, weak specimen

withstood higher stresses beyond the initial peak, as shown in Fig. 7. Thus, the material appeared to strengthen as it was crushed. It is postulated that material variations in the foaming direction caused the apparent strengthening of these samples. It is a challenge to produce perfectly uniform foams due to gravity-dependent settling effects than can slightly alter the homogeneity of the material prior to solidification. The foam tested in the against-rise direction was likely more uniform since there were no settling effects during processing. The distinct strength behaviors observed for the WR specimens are a natural result of foaming during the manufacturing process. It should also be noted that the foams tested here are continually improving as part of this team project. Goals of this project include advancing the manufacturing process concerning quantity (e.g., foam billet size) and quality (e.g., property uniformity) while maintaining reasonable production costs.

The compressive strengths as a function of bulk density are shown in Fig. 8 for samples tested in both the WR and the AR directions. The strength was defined as the first peak of the stress-strain curve. The equations for the best fit of the data are also included in Fig. 8. Both the AR and the WR samples exhibited a power law relationship between strength and density. The WR data was best fit by an equation with an exponent of 1.4, while the equation representing the AR data had an exponent of 1.6. The WR data also had more scatter (an R^2 value of 0.82, compared with an R^2 value of 0.95 for AR samples). The Gibson-Ashby relationship for open-cell, brittle foams somewhat similar to the graphite foams tested here, predicted that the crushing strength (σ^*_{cr}) should be related to

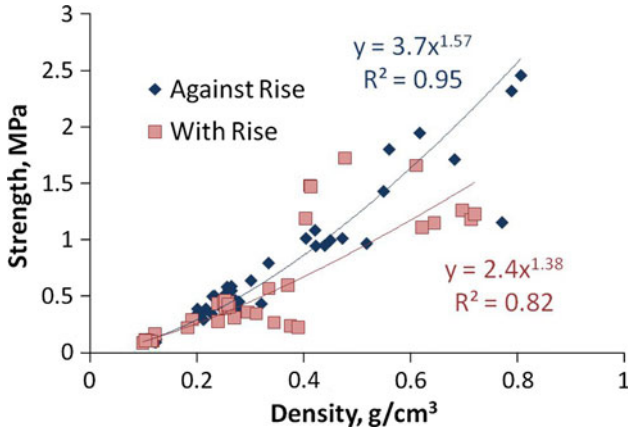

Fig. 8 Compressive strength versus bulk density for foam tested in the WR and AR directions

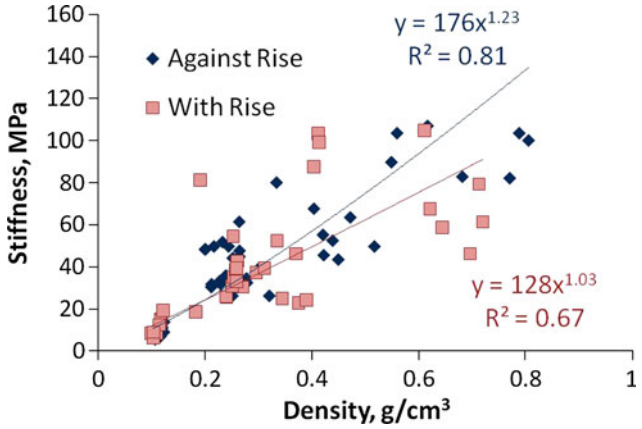

Fig. 9 Compressive modulus versus density

density (ρ*) by a power law with an exponent of 1.5, according to the following equation:

$$\frac{\sigma^*_{cr}}{\sigma_{fs}} \propto \left(\frac{\rho^*}{\rho_s}\right)^{3/2} \quad \text{(Eq 1)}$$

where σ_{fs} is the modulus of rupture of a strut (related to fracture toughness: an unknown quantity in this situation) and ρ_s is the density of the solid material (Ref 7). The constant of proportionality is typically 0.2. The AR samples in this study (with an exponent of 1.6 and less statistical variation) fell more in line with the G-A model than the WR samples. At low densities (less than 0.5 g/cc) the strength of the WR samples was consistent with the AR samples. It was at the higher densities that the WR samples deviated from the anticipated strength.

The compressive moduli showed significant scatter when plotted as a function of density (Fig. 9). In general, the lowest density samples had the lowest moduli, but beyond 0.2 g/cm^3 the data showed little trend. Note that the stiffness reported here corresponds to the second linear region of the stress-strain curve and was obtained by linear regression fit.

4. Conclusions and Future Directions

Due to the lack of deformation/strength data regarding this relatively new material system, an extensive characterization campaign was initiated. Here, procedures were developed to study the compressive behavior and to start building a data base for the GTIH graphite foam material. As expected for this brittle graphite foam material, there was quite a bit of statistical variability in both moduli and strength indicating the need for stochastic modeling approaches. Another important observation involved the intra-specimen density variations, especially in the WR direction. These density variations caused two types of failure behaviors in the WR data set. Specimens with uniform densities were stronger and had a flatter post crush stress-strain responses. Specimens with more pronounced density variations were weaker (as defined by stress at crush initiation) and had peaks and valleys during continued crushing. This signified progressive failure of weak (i.e., low density) regions. Full field optical strain measurement data showed that the material compresses uniformly until reaching a critical stress at which individual layers begin to successively collapse. As the project evolves, testing will continue on the still improving materials fabricated by GTIH. Experiments addressing tensile properties are currently being conducted.

Acknowledgments

The authors would like to thank Dr. Ajit Roy (Technical Monitor and Sr. Material Research Engineer at AFRL) and Dr. Alan Janiszewski (Vice President for Materials & Manufacturing at Universal Technologies Corp.) for their guidance and funding of this project under U.S. Air Force contract FA8650-05-D-5807. In addition, the authors wish to thank Dr. Peter Stansberry and GTIH for supplying the graphite foam samples.

References

1. J. Klett, R. Hardy, E. Romine, C. Walls, and T. Burchell, High-Thermal-Conductivity, Mesophase-Pitch-Derived Carbon Foams: Effect of Precursor on Structure and Properties, *Carbon*, 2000, **38**(7), p 953–973
2. J. Klett, Carbon Foams, *Cellular Ceramics*, M. Sheffler and P. Colombo, Ed., Wiley, New York, 2005, p 137–157
3. W. Lin, A Review of Graphite Foam as Thermal Material, Project Report, Lund, Sweden, May 12, 2010
4. A. Gyekenyesi, M. Singh, C. Smith, P. Stansberry, M. Alam, and D. Vrable, Development and Characterization of High Conductivity Graphite Foams for Thermal Management Applications, *Ceramic Engineering and Science Proceedings—Advanced Materials for Sustainable Developments, CESP*, Vol 9, H.T. Lin, A. Gyekenyesi, L. An, S. Mathur, and T. Ohji, Ed., Wiley, New York, 2010, p 75–81
5. "Standard Test Method for Flexural Strength of Advanced Ceramics with Engineered Porosity (Honeycomb Cellular Channels) at Ambient Temperatures," C1674-08, ASTM Standard, 2008
6. R. Brezney and D. Green, Uniaxial Strength of Brittle Cellular Materials, *J. Am. Ceram. Soc.*, 1993, **76**(9), p 2185–2192
7. M.F. Ashby, Cellular Solids—Scaling of Properties, *Cellular Ceramics*, M. Sheffler and P. Colombo, Ed., Wiley, New York, 2005, p 3–16
8. L.J. Gibson and M.F. Ashby, *Cellular Solids—Structure and Properties*, 2nd ed., Cambridge University Press, Cambridge, 1997, p 175–231
9. P. Stansberry, E. Pancost, Y. Xiong, and J. Norley, Graphite Foam Performance in Heat Exchanger Applications, *Proceedings of SAMPE Fall Technical Conference*, Wichita, Kansas, October 19–22, 2009, p 101–110